

1 **Comparison of colloidal silica involved fouling behavior in three membrane**
2 **distillation configurations using PTFE membrane**

3 Wenli Qin^{a,c}; Zongli Xie^{a,*}, Derrick Ng^a, Ying Ye^c, Xiaosheng Ji^c, Stephen Gray^b,
4 Jianhua Zhang^{b,*}

5
6 a. CSIRO Manufacturing, Private bag 10, Clayton South MDC, Vic. 3169, Australia

7 b. Institute for Sustainability and Innovation, Victoria University P.O. Box 14428, Melbourne,
8 Vic 8001, Australia

9 c. Institute of Marine Geology and Resource, Ocean College, Zhejiang University, Zhoushan,
10 Zhejiang 316021, China

11 **Abstract:**

12 Colloidal silica involved fouling behaviors in direct contact membrane distillation
13 (DCMD), vacuum membrane distillation (VMD) and sweeping gas membrane
14 distillation (SGMD) were studied. Three foulants were used in the experiments,
15 including colloidal silica as representative of particulate foulants, calcium bicarbonate
16 as dissolved inorganic foulant, and NOM (humic acid + alginate + BSA) as the
17 dissolved organic foulant. The three types of foulants were combined to produce four
18 different feed waters: silica alone; silica + calcium bicarbonate; silica + NOM; and
19 silica + calcium bicarbonate + NOM. With 25% feed recovery, it was found that VMD
20 showed the worst performance for most of the foulant combinations due to turbulence

21 dead zones caused by the membrane deformation that increased foulant deposition.
22 For the silica + calcium bicarbonate + NOM feed DCMD had the greatest fouling rate,
23 although DCMD also had the highest flux of all configurations. SGMD showed the best
24 fouling resistance of all configurations, although it was inclined to calcium carbonate
25 fouling because carbon dioxide was removed in the permeate leading to calcium
26 carbonate precipitation and could be alleviated by using air as sweeping gas. For feeds
27 containing high-concentration calcium bicarbonate or carbonate foulants, VMD should
28 be avoided to lower the formation of carbonate precipitants on the membrane surface if
29 scale inhibitors are not used.

30

31 Key words: Membrane distillation; membrane fouling; colloidal silica; MD
32 configuration

33 **1. Introduction:**

34 Membrane distillation (MD) is a hybrid of thermal distillation and membrane
35 separation described in technical literature since 1967 (Banat et al. 2002, Lawson and
36 Lloyd 1997, Lei et al. 2005, Weyl 1967). Although a membrane is involved in MD, the
37 driving force is quite different from other membrane processes, being the vapour
38 pressure difference across the membrane which drives mass transfer through a
39 membrane (Lawson and Lloyd 1997, Schneider and van Gassel 1984), rather than an
40 applied pressure difference, a concentration gradient or an electrical potential gradient.

41 MD has 100% theoretical rejection to non-volatile components and is proposed to

42 be utilised with low grade heat sources of 40-80°C (Zhang et al. 2010b). Since the
43 driving force of MD is a partial vapour pressure difference across a membrane
44 commonly triggered by a temperature difference, its flux is not likely sensitive to feed
45 salinity in practical water treatment. Therefore, MD can be combined with conventional
46 reverse osmosis (RO) processes to increase water recovery and minimise high
47 concentration brine discharge. Therefore, MD can combine with conventional reverse
48 osmosis (RO) processes to minimise high concentration brine discharge. However, to
49 achieve high RO recovery in zero liquid discharge processes, the RO concentrate will
50 be nearly saturated or saturated by some low solubility inorganic and organic salts, such
51 as humic acid, calcium bicarbonate, and colloidal silica, which are major foulants for
52 membrane process. Although MD shows much better fouling resistance than RO, it still
53 suffers from fouling problems (Gryta 2008, Warsinger et al. 2015). Membrane fouling
54 in MD will reduce productivity, deteriorate permeate quality, increase energy
55 consumption and treatment cost, shorten membrane life span , and even cause
56 membrane wetting (Qin et al. 2017).

57 PTFE membrane has desirable characteristics for use in membrane distillation. The
58 PTFE has high hydrophobicity with surface energy of 9.1 kN/m (Mulder 1996). Its
59 thermal conductivity is as low as 0.22-0.45 Wm⁻¹K⁻¹ and has excellent chemical
60 stability at the operating temperatures of membrane distillation (Alklaibi and Lior
61 2005). Furthermore, the porosity of PTFE membrane can be as high as 90% (Zhang et
62 al. 2010a). However, the PTFE membrane is not as rigid as PVDF membrane and can
63 be deformed easily under pressure which will affect its performance (Zhang et al. 2011).

64 In MD processes, one side of the membrane contacts the liquid feed. Depending on
65 the permeate collection design, four MD configurations are generally recognised:
66 DCMD, Air Gap Membrane Distillation (AGMD), VMD and SGMD (Alklaibi and Lior
67 2005, Zhang et al. 2013b). While these processes operate in a similar manner, they have
68 different operating characteristics with DCMD usually resulting in higher flux but
69 lower thermal energy efficiency, and AGMD higher thermal energy efficiency but
70 lower flux (Lei et al. 2005).

71 Previous MD fouling studies have generally considered only one particular MD
72 configuration (Qin et al. 2017, Wang et al. 2016a, Wang et al. 2016b), and there has
73 been little research focused on comparison of fouling behaviour of MD configurations,
74 especially for feeds containing colloidal silica. In this study, the performance of the
75 DCMD, SGMD and VMD were studied using synthetic feeds with different types of
76 foulant combination. Furthermore, the influence of PTFE membrane compression on
77 fouling behaviours is also discussed. While AGMD is more commonly considered than
78 SGMD, we have previously found that the gap distance in AGMD is very hard to
79 control experimentally when flexible PTFE membrane is used. While other researchers
80 have not reported such experimental issues, we have been concerned with the
81 membrane directly contacting the cooling plate and affecting the fouling behaviour.
82 Furthermore, this configuration is very complex for fabrication, and permeate can build
83 up in the gap leading to operation as permeate gap membrane distillation. Therefore,
84 flowing air was used to keep the channel clear of liquid.

85 In this study, we focused on the influence of permeate collection methods in

86 different configurations on the feed side fouling, which was rarely researched but
87 important for MD commercialisation.

88 **2. Materials and Method:**

89 *2.1 Materials*

90 A hydrophobic, microporous membrane from Changqi Ltd. (Ningbo, China) was
91 used in the MD experiment. The membrane consisted of a thin polytetrafluoroethylene
92 (PTFE) active layer (thickness 30 μm) on top of a polypropylene (PP) support layer
93 with a total membrane thickness of 120 μm . The nominal pore size and porosity of the
94 PTFE active layer were 0.5 μm and 90 %, respectively.

95 Ludox HS-40 silica colloids (particle size = 12 nm) from Sigma-Aldrich were used
96 to represent a colloidal/particulate foulant; humic acid (Sigma-Aldrich), alginate
97 (Sigma-Aldrich) and bovine serum albumin (BSA, Sigma-Aldrich)) were used to
98 represent natural organic matter; calcium carbonate was used as the dissolved inorganic
99 foulant synthesized by calcium chloride and sodium bicarbonate. A stock solution (5 g
100 L^{-1}) with each organic foulant was prepared by dissolving each organic foulant into
101 Milli-Q water and stored in a sterilized amber glass bottle at 4°C. The Ludox HS-40
102 colloidal silica suspension (40 wt. %) was sonicated for 10 min to ensure complete
103 dispersion before adding to the feed solution. All the feeds contained NaCl (1 mol/L)
104 and colloidal silica (1000 mg/L), and depending on the combination, also contained
105 $\text{Ca}(\text{HCO}_3)_2$ (648mg/L) and/or natural organic matter (NOM) that consisted of humic
106 acid (200 mg/L), alginate (200 mg/L), and BSA (200 mg/L).

107

2.2 Membrane testing

108 Figure 1 shows a schematic of the laboratory MD system which consisted of a flat
109 sheet membrane module made from acrylic blocks, a feed tank, a permeate tank, a
110 circulating pump and/or a vacuum pump. The membrane was placed in the middle of
111 the module with an effective membrane area of 65 cm^2 (membrane dimension $5 \text{ cm} \times 13$
112 cm). Spacers (thickness = 0.7 mm , filament diameter = 0.35 mm , porosity = 0.87) were
113 placed on both sides of the membrane to enhance the turbulence of the streams and
114 guide the flow in the membrane module. The channel depths were 1 mm where the
115 spacers were placed. The temperature of the feed solution was maintained by a water
116 bath (DF-101S, Yuhua Instruments). The initial feed volume of different MD
117 configurations was kept constant at 2 litre . In DCMD mode (Figure 1a), the stream
118 velocities on both sides of the membrane were kept equal at 0.56 m/s (flow rate = 500
119 mL/min) and controlled by two Masterflex peristaltic pumps. An ice water cooler was
120 used to cool the permeate stream and the temperature was maintained at 10°C for all
121 experiments under the stable conditions. The temperatures at the inlets and outlets of
122 both the feed and permeate streams were monitored using K-type thermocouples and
123 the weight gain of the permeate tank on the permeate side was continuously recorded
124 every 5 seconds using an electronic balance ($\pm 0.1 \text{ g}$ accuracy, model GF-6000, A&D
125 Instruments) connected to a data logger. The water flux was determined via the weight
126 gain of the permeate reservoir per unit area over time (5 min) and is expressed as
127 $\text{L/m}^2 \cdot \text{h}$. The run time was about 6 h .

128 For SGMD (Figure 1b) and VMD systems (Figure 1c), the weight loss of the feed
129 tank on the feed side was continuously recorded every 5 seconds using an electronic
130 balance connected to a data logger. In SGMD system, nitrogen (N₂) was used to strip
131 the permeate from the feed and the flowrate was maintained at 7 L/min (2.33 m/s) and
132 monitored by a flowmeter. The run time was about 20 h. In the VMD system, a vacuum
133 pump was utilized to produce vacuum pressure of 1.33 kPa (10 torr) and the permeate
134 was condensed by chilled water at 5°C in a container prior to the vacuum pump. The
135 run time was about 10 h. On the feed sides of SGMD and VMD, the inlet temperature
136 and flow velocity were maintained to be the same. The water flux was determined via
137 the weight gain or loss of permeate (for DCMD) or weight loss of feed (for SGMD and
138 VMD) reservoir per unit area over time and is expressed in the units of L/m²·h. The
139 feed tank was covered by preservative film to prevent losing water by evaporation
140 during the test.

141 MD fouling experiments were conducted for DCMD, SGMD and VMD
142 configurations. A new membrane specimen was used for each experiment. Every test
143 was repeated at least for three times, and the results presented in this paper were the
144 average values of the three repeats. Although the initial flux variation for each repeat
145 was about ±5% due to the difference among the new membrane specimens, the flux
146 decline trends were similar between the repeats. In addition, all the experiments were
147 purposely terminated at the same water recovery rate of 25%, so the fouled membrane
148 at the end of the experiment can be compared on the same basis.

149 Conductivity of the permeate stream was measured by a conductivity meter (CON
150 110, Oakton Instruments) every 30 minutes for DCMD, and every 120 minutes for
151 SGMD and VMD. After each fouling test, the membrane was removed from the
152 membrane cell and was kept in a desiccator for subsequent characterisation.

153 For each experiment, the minimum recovery calculated by Equation (1) was 25%.

$$154 \quad Rec = \left(1 - \frac{m_t}{m_0}\right) \times 100\% \quad (1)$$

155 where Rec is the feed recovery and m_0 and m_t are the initial feed mass and mass of feed
156 at time t respectively.

157 The salt rejection was calculated by Equation (2).

$$158 \quad Rej = \left(1 - \frac{C_{permeate}}{C_{feed}}\right) \times 100\% \quad (2)$$

159 where Rej is the salt rejection, $C_{permeate}$ and C_{feed} are the conductivities of the feed and
160 permeate, respectively.

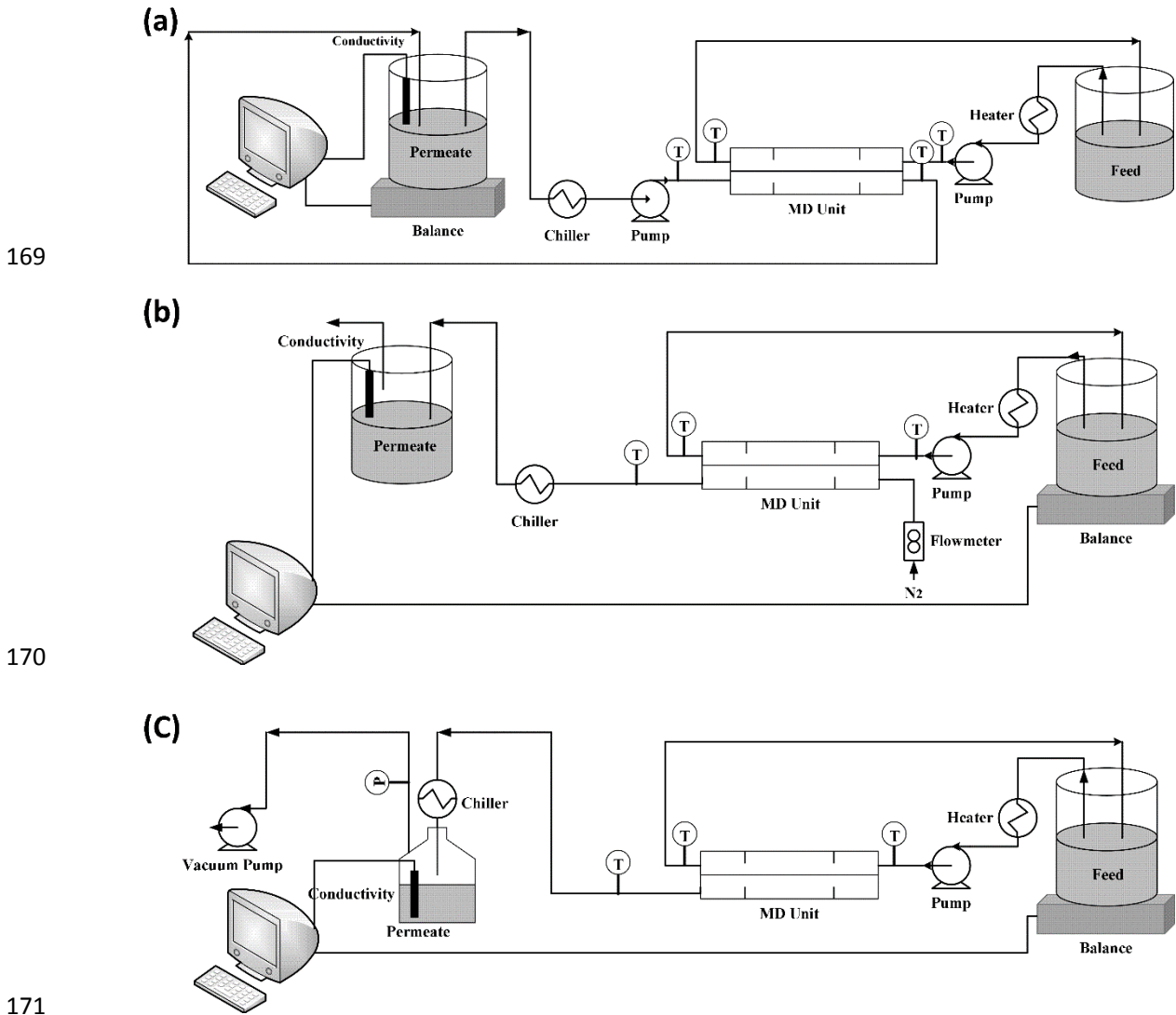
161 For spacer filled flow channels, the local Reynolds number can be computed by
162 (Geankoplis 2003, Phattaranawik et al. 2001, Zhang et al. 2012),

$$163 \quad Re = \frac{\rho d_h v}{\mu} \quad (3)$$

164 Here, ρ is the water density, v is the linear velocity of the feed, μ is the water
165 viscosity and d_h is the hydraulic diameter in a spacer filled channel and is calculated by

$$166 \quad d_h = \frac{4.0 \varepsilon_s d_f h_s}{2d_f + 4(1 - \varepsilon_s)h_s} \quad (4)$$

167 Here, ε_s is the spacer porosity, d_f is the spacer filament diameter, and h_s is the spacer
168 thickness.



172 Figure 1 MD set up in the lab: (a) DCMD, (b) SGMD, (c) VMD.

173 *2.3 Analytical methods*

174 The morphology of the fouling layer deposited onto the membrane surface was
175 examined by a scanning electron microscope (SEM, Zeiss Merlin FESEM). Both
176 membrane surface and cross sectional images were taken. Distribution of fluorine (F),

177 carbon (C), calcium (Ca), sodium (Na), and silica in the fouled membrane cross section
178 was mapped by energy-dispersive X-ray spectroscopy (EDS, Zeiss Merlin FESEM).

179 **3. Results and discussions:**

180 *3.1 DCMD, VMD and SGMD fouling tests*

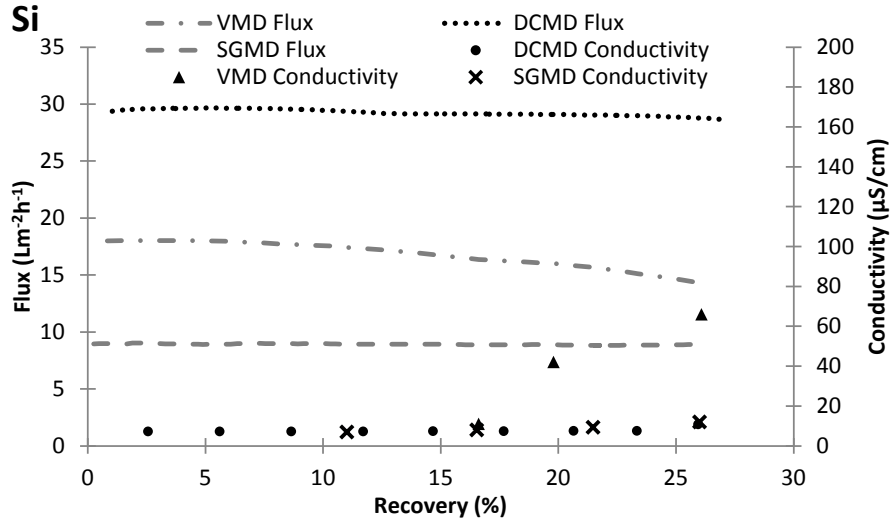
181 *3.1.1 Performance of different configuration*

182 Based on Figure 2 and Table 1, the same foulant combinations had quite different
183 influences on the flux decline magnitudes of the different MD configurations. With 25%
184 feed recovery, the silica only feed had very little influence on DCMD (2.5% decline)
185 and SGMD (1.7% decline) fluxes, but caused about 20.4% flux decline of VMD.

186 Silica+Ca combination showed little influence on the DCMD flux when the
187 recovery was less than 23%, and led to about 8.9% flux decline with 25% recovery.
188 However, for SGMD and VMD, Silica+Ca combination showed a stronger influence
189 on flux than that of DCMD, and caused 11.7% and 25.2% flux decline respectively for
190 25% recovery.

191 Si+NOM combination also had very little influence on SGMD flux (1.2% flux
192 decline), but caused about 20.6% flux decline of VMD and 16.7% flux decline of
193 DCMD.

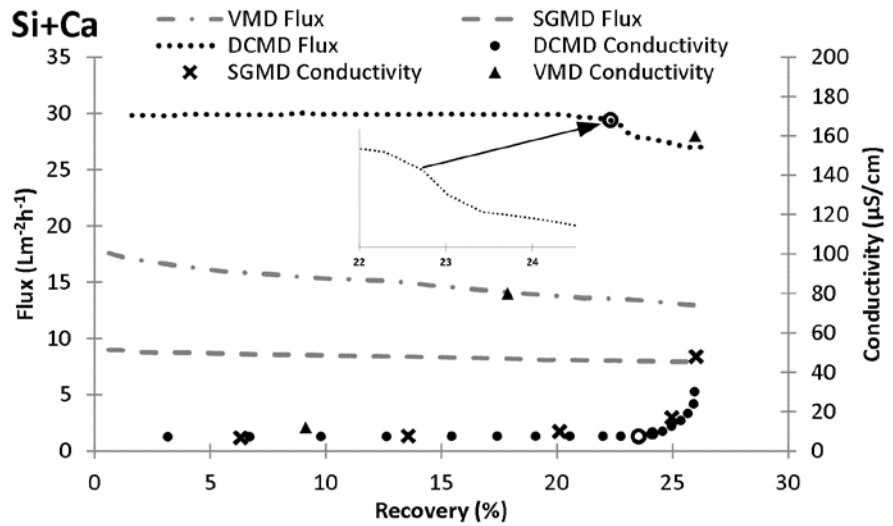
194 At 25% recovery, it can be seen in Table 1 that the Si+Ca+NOM combinations
195 showed the worst fouling to all configurations. DCMD showed the least resistance to
196 this foulant combination and had a flux decline about 51.4%. SGMD and VMD had
197 flux decline 14.4% and 30.4% respectively.



198

199

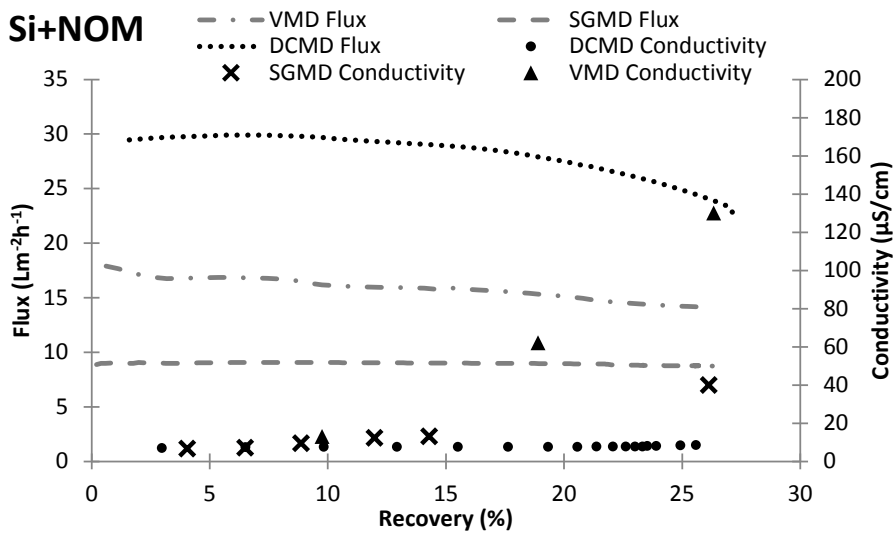
(a) Silica



200

201

(b) Silica and Ca(HCO₃)₂

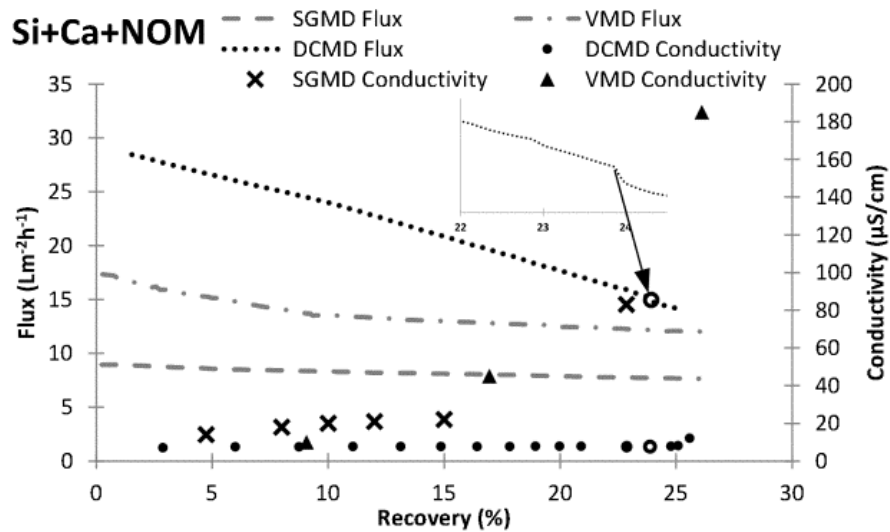


202

203

(c) Silica and NOM

204



205

206

(d) Silica, $\text{Ca}(\text{HCO}_3)_2$ and NOM

207

Figure 2. Water flux and permeate conductivity as a function of water recovery

208

during membrane distillation fouling in different configurations (DCMD: feed inlet

209

temperatures = 40°C and permeate inlet temperature = 10°C, feed and permeate

210

velocities were 0.56 m/s in countercurrent mode; SGMD: feed inlet temperatures =

211

40°C, N_2 velocity = 2.33 m/s (7 L/min); VMD system, the vacuum pressure = 1.33 kPa).

212

Table 1. Percentage of flux decline at 25% recovery (experimental error $\pm 5\%$)

Foulants	Flux Decline		
	(%)		
	DCMD	SGMD	VMD
Si	2.5	1.7	20.4
Si + Ca	8.9	11.7	25.2
Si + NOM	16.7	1.2	20.6

Si + Ca+ NOM	51.4	14.1	30.4
--------------	------	------	------

213 *3.1.2 Discussion of the fouling behaviors in different configurations*

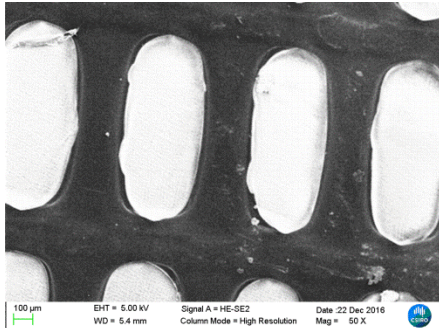
214 Table 1 shows that at 25% water recovery, DCMD showed the highest percentage
215 flux decline (51.4%) with the Si+Ca+NOM feed, and VMD showed the highest rates
216 of fouling for the all other foulant combinations although DCMD constantly showed
217 the highest initial fluxes in all tests. This phenomena is not consistent with traditional
218 fouling theory, in which high flux is prone to increase fouling issues for the same
219 hydrodynamic conditions due to the high concentration polarisation in the boundary
220 layer (Bacchin et al. 2006, Chen et al. 1997).

221 Since the feed side hydrodynamic conditions were similar in all the tests, the reason
222 is most likely to arise from changes in membrane property for VMD configuration.
223 PTFE material can be deformed under strain or compression (Rae and Brown 2005, Rae
224 and Dattelbaum 2004). The PTFE membrane used in the test had porosity of
225 approximately 90%, and was supported by scrim as shown in Figure 3(a) (Zhang et al.
226 2010a). Membrane compaction under high compression pressure can lead to a loss of
227 the membrane permeability, although initially membrane permeability increase was
228 found under low compression pressure (Lawson et al. 1995, Zhang et al. 2012). In
229 Figure 4, schematic diagrams for PTFE membrane in different configurations are shown.
230 It can be seen that the pressure on both sides of the membrane is balanced in DCMD
231 and SGMD. Therefore, although PTFE is very soft material and the membrane porosity
232 is about 90%, the membrane surface will not be deformed and pressed into the

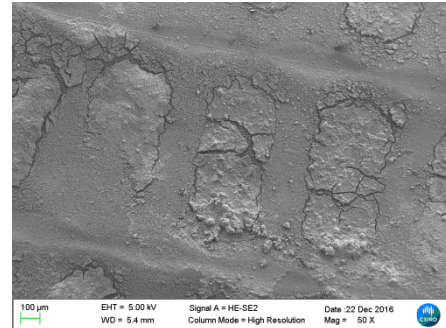
233 supporting scrim. However, in VMD, the unbalanced pressure (hydraulic pressure + the
234 vacuum pressure > 1 bar) applied only on one side of the PTFE membrane and was able
235 to push the soft PTFE membrane into the void space of the scrim. The deformation of
236 membrane can be observed by Figures 3(b), 3 (d), and all the following SEM images
237 of the membrane cross section used in the VMD. Therefore, although the feed flow
238 channel of the MD process was filled with spacer to increase turbulence ($Re = 954$) and
239 reduce temperature polarisation and membrane fouling (Zhang et al. 2012), the
240 deformed section in VMD formed tiny static quiescent zone or dead zones as shown in
241 Figure 3(b) reduced the turbulence effect of the spacer and encouraged the formation
242 of the fouling layer and increase temperature polarisation. It also can be found from
243 Figures 3(c) and (d) that the foulant accumulated in the concaved section. The nominal
244 driving force (vapour pressure difference) across the membrane of VMD and DCMD
245 were all about 6 kPa respectively based on the Antoine equation (Zhang et al. 2010a).
246 However, the VMD initial flux was only about 60% of that of DCMD, which can be
247 explained by increased temperature polarisation and membrane compression (Lawson
248 et al. 1995, Zhang et al. 2013a, Zhang et al. 2012).

249 It also can be seen in Table 1 that the foulant combinations were also key factors
250 that determine the extent of fouling, and it is proposed that the extent of fouling can be
251 determined by either flux or turbulence effects. For the VMD and SGMD, both low flux
252 configurations, the Si+NOM combination showed almost the same influence on flux as
253 the Si feed. However, the Si+NOM combination caused the second highest flux loss
254 (16.7%) for higher flux DCMD operation at 25% recovery. Therefore, the addition of

255 NOM led to fouling was more flux or flux incurred concentration polarisation
256 dependent than turbulence dependent, since NOM was solute in the feed. In contrast,
257 silica fouling was more turbulence dependent than flux or flux incurred concentration
258 polarisation dependent due to its particulate properties, as identified by the higher flux
259 loss for VMD upon deformation of the membrane. The combination of the three
260 foulants enhanced both the flux/concentration polarisation (DCMD) and turbulence
261 (VMD) dependences of the fouling process, due to the interactions between these
262 foulants (Kitano et al. 1969, Laqbaqbi et al. 2017, Qin et al. 2017). Furthermore, it can
263 be seen from Table 1, the enhancement of dependence was more pronounced on
264 flux/concentration polarisation than turbulence by comparing DCMD with VMD for
265 combinations of three foulants.

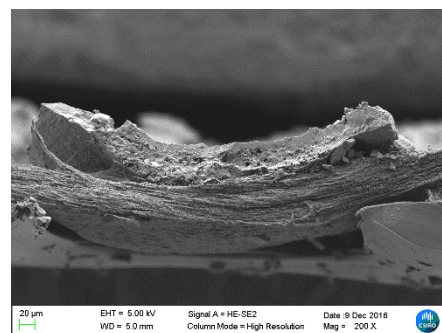
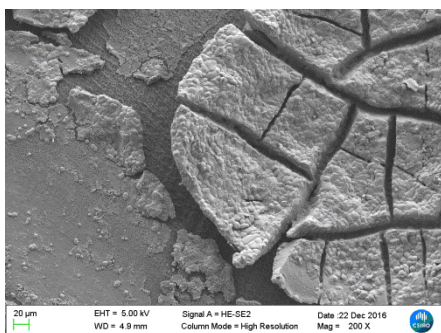


266
267 (a) Scrim



(b) Concave membrane surface

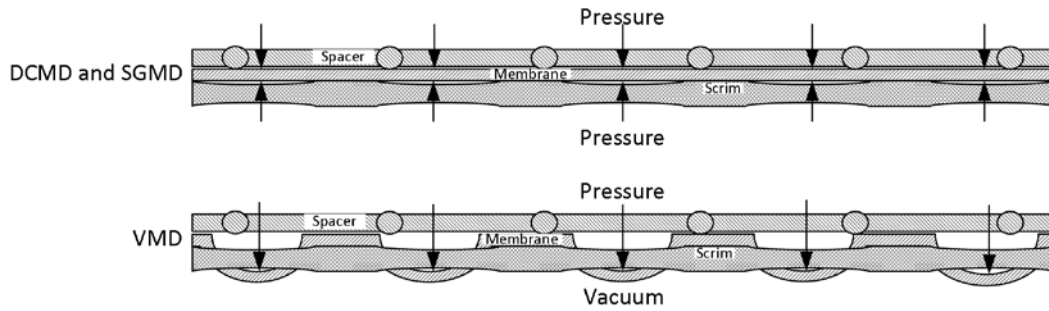
268 following VMD operation



269

270 (c) Foulant in the concaved section (d) Cross-section of the concaved
 271 following VMD processing section following VMD operation

272 Figure 3. Concaved sections of VMD membrane



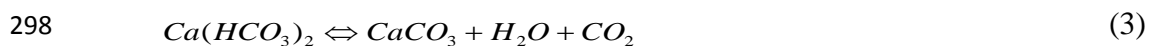
273

274 Figure 4. Schematic diagrams for PTFE membrane in different configuration

275 From Table 1, it is also found that calcium carbonate fouling showed less influence
 276 on DCMD flux than that of VMD and SGMD. This was mainly caused by the faster
 277 decomposition of the dissolved $Ca(HCO_3)_2$ in VMD and SGMD than that of DCMD,
 278 which eventually formed $CaCO_3$. The equilibrium of $Ca(HCO_3)_2$ vs $CaCO_3$ is shown
 279 in Eq. (3). If CO_2 in Eq. (3) is removed from the system, the equilibrium will favour
 280 the formation of $CaCO_3$. The feed during the test would reach an equilibrium under
 281 atmospheric pressure and the CO_2 concentration would be about 0.04% (Ballantyne et
 282 al. 2012). Unlike DCMD where the permeate side was also saturated with CO_2 , the
 283 permeate sides of VMD and SGMD (pure nitrogen) contained negligible amount of
 284 CO_2 . Therefore, the mass transfer driving force of CO_2 across the membrane was higher
 285 in VMD and SGMD than in the DCMD, and the continuous removal of CO_2 from the
 286 feed during VMD and SGMD shifted the equilibrium to the formation of $CaCO_3$ and a
 287 fouling layer on the membrane surface (Frear and Johnston 1929).

288 This proposition could not be well supported by the lowering pH (about 5.6) on the

289 permeate side, since the ionic strength was low and the values shifted with time.
290 However, it can also be supported by conductivity variations during those tests, despite
291 the nominal salt (NaCl) rejections calculated by Eq. (2) being higher than 99.9% for all
292 tests. It can be seen from Figure 2a and 2c for the feed that only contained Si foulant
293 and Si+NOM, the permeates from DCMD and SGMD only had slight conductivity
294 change, but for VMD its permeate conductivity increased continuously due to the CO_2
295 depletion from the feed to the permeate side. Furthermore, the permeate conductivity
296 for the VMD tests increased to greater than 100 $\mu\text{S}/\text{cm}$, which also suggested that
297 wetting occurred in VMD (Enrquez et al. 2013, Gajevskiy 2015, Light et al. 1995).



299 It is also interesting to observe that in DCMD for both calcium containing feeds,
300 there were quick flux decline rate changes which occurred almost at the same recovery
301 22.5-23.5% (shown as hollow dot points in Figures 2b and 2d), accompanied with
302 conductivity increases. This phenomenon was caused by the concentration increase of
303 $Ca(HCO_3)_2$ due to the recovery increase, which would also cause CO_2 increase in the
304 feed as shown in Eq. (3). When the concentration of CO_2 in the feed was higher than
305 that in the permeate, the CO_2 would start transferring into the permeate and cause the
306 permeate conductivity to increase. Since the CO_2 transferred from the feed to the
307 permeate and its concentration reduced in the feed, the equilibrium as shown in Eq. (3)
308 moved to the $CaCO_3$ formation side. Thus, the rapid flux decline was observed. Similar
309 phenomenon can also be found in SGMD, and fast conductivity increase was observed
310 at about 22% feed recovery, but it was not very obvious in VMD, because of the high

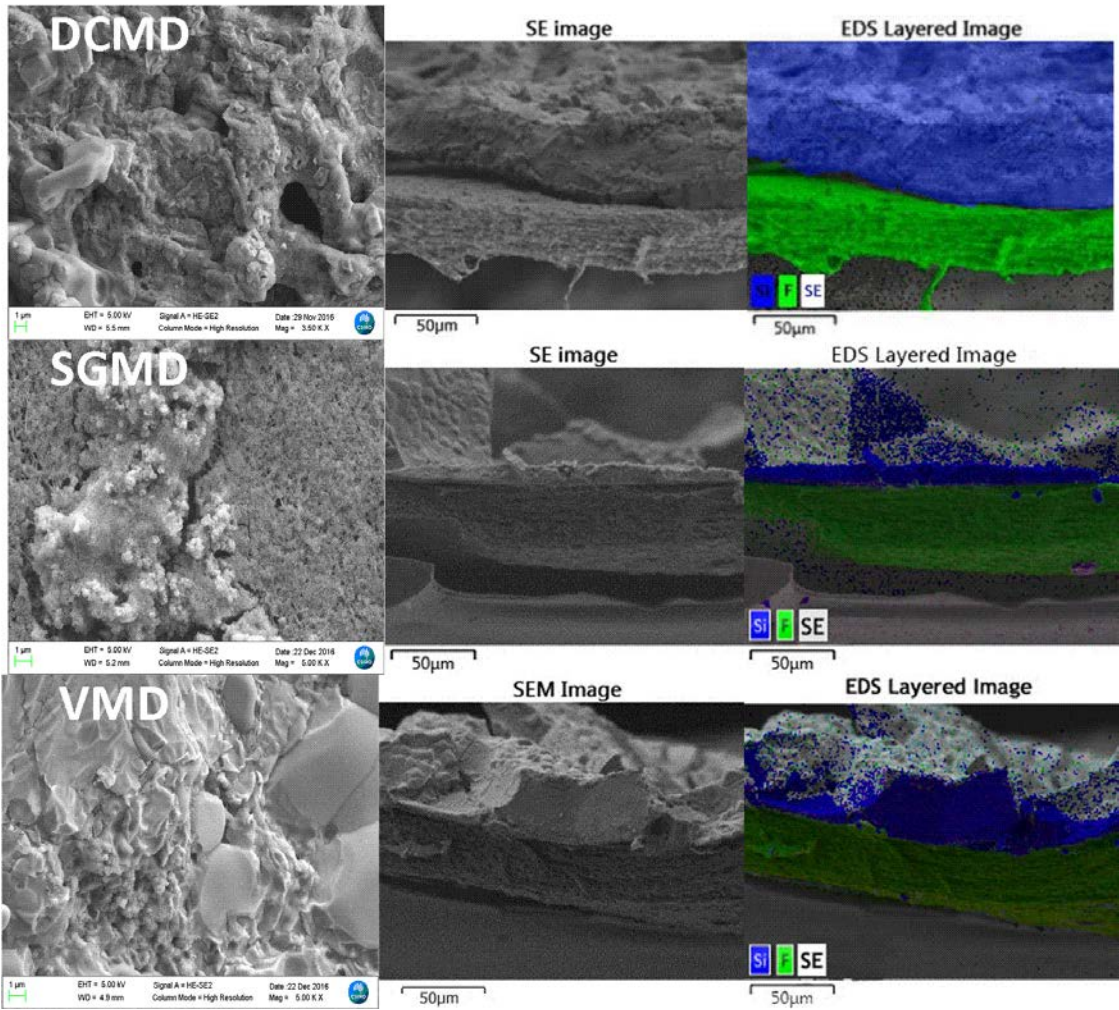
311 mass driving force of CO_2 and the continuous decomposition of $Ca(HCO_3)_2$.

312 *3.1.3 Surface morphology of the fouled membrane*

313 SEM and EDS images of the fouled membrane are shown in Figure 5. For the silica
314 only feed (Si), it can be observed in Figure 5(a) that both the fouling layers formed on
315 the DCMD and SGMD were more porous than that of VMD, which caused less flux
316 decline rate than that of VMD (Table 1). However, it is hard to see the difference in
317 detail from the cross section of the fouling layer in Figure 5(a), except for the VMD, in
318 which an accumulated fouling layer was observed in the deformed section of the PTFE
319 membrane.

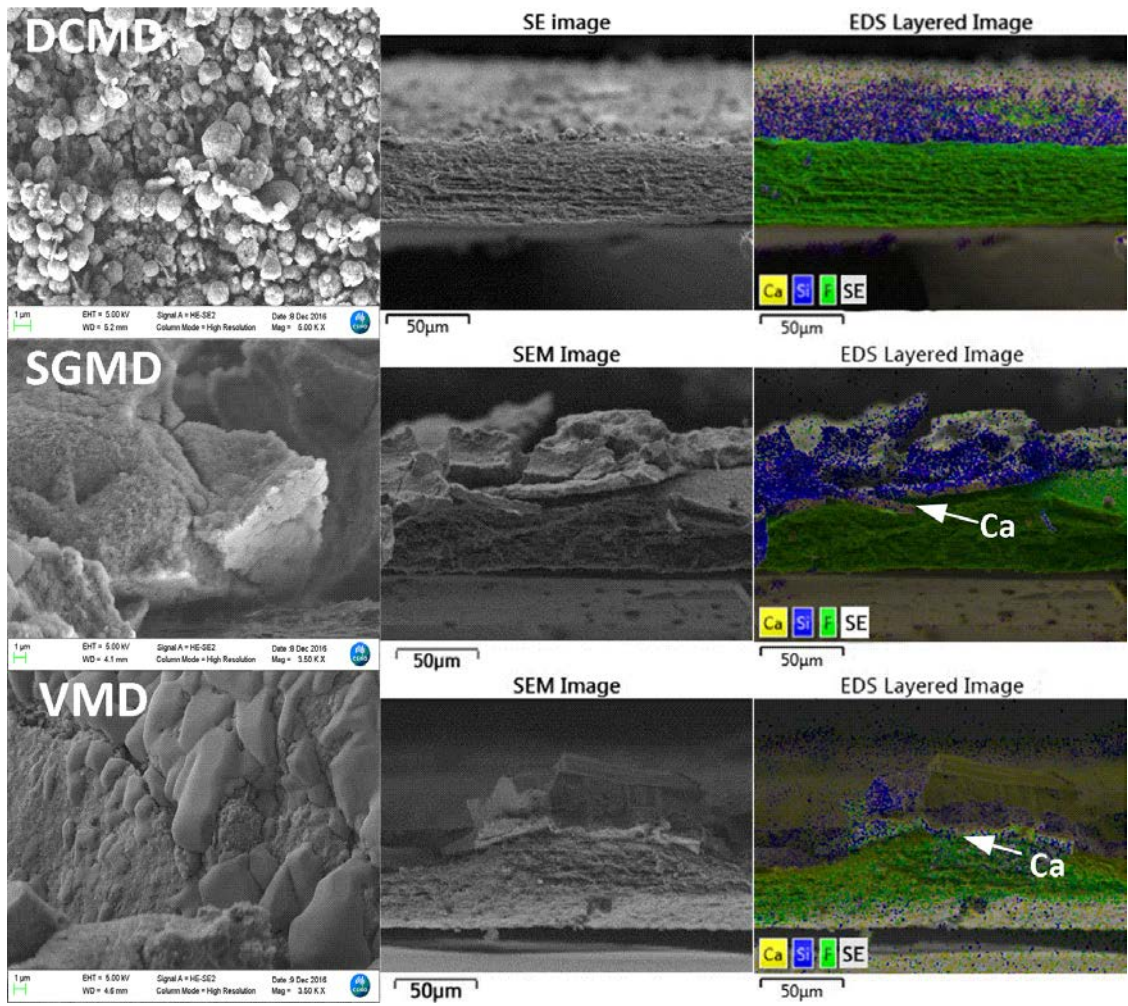
320 Another interesting note is that, for the calcium containing silica feed (Si+Ca),
321 some spherical foulant formation was observed on the top of membrane surface in
322 DCMD, this formation is specific to DCMD as it was not present on membrane surfaces
323 in VMD and SGMD configurations. The spherical foulant (Figures 5b, 5c and 5d) was
324 calcium carbonate as suggested by others (Trushina et al. 2015, Yu et al. 2004). It can
325 be seen from Figure 2(b) that a flux decline in DCMD occurred at about 22-24%
326 recovery, which was caused by the supersaturated calcium carbonate precipitating from
327 the bulk feed and forming a calcium carbonate layer on top of the silica fouling layer.
328 However, for the VMD and SGMD processes, it is shown in Figure 2(b) that the flux
329 almost declined continuously. Therefore, the formation of calcium carbonate fouling
330 layer commenced from beginning of the tests, which was also demonstrated by EDS of
331 Figure 5(b) where the calcium was found at the bottom of the fouling layer in SGMD
332 and VMD, but only found the mostly on the top of fouling layer in DCMD.

333 For the NOM containing silica feed, the membrane surface and cross sectional
334 SEM images for the different MD configurations are shown in Figure 5(c). It can be
335 found in DCMD that a dense flat fouling layer formed on the membrane (Figure 5(c))
336 and the bright red carbon containing layer (EDS, Figure 5(c) in the circle) formed
337 directly on surface of the membrane (by comparing the SEM image in the circle) under
338 a silica dominated fouling layer due to the high flux /concentration polarisation
339 dependence of NOM. However, the fouling layers (Figure 5(c)) for SGMD and VMD
340 were not as smooth as that for DCMD. Furthermore, the carbon element was likely
341 distributed on top of the silica dominated fouling layer for SGMD and distributed
342 evenly and relative sparsely in the fouling layer of the silica dominated layer. Based on
343 the EDS images, it can be found that NOM fouling dominated at the highest flux stage
344 (the early stage) in DCMD prior to silica fouling, and formed at almost same time with
345 or later than silica fouling in VMD, and only was found on the fouling layer surface in
346 SGMD. The carbon found on the fouling layer in SGMD should not be a fouling layer
347 and but contamination from the residual feed solution, since the NOM has an
348 amorphous structure (Lee et al. 2004) rather than a crystal structure as shown in Figure
349 5(c) SGMD image. Therefore, NOM fouling formation seems more sensitive to high
350 flux and concentration polarisation rather than that of low turbulence, since the VMD
351 has the least turbulence in all configurations due to the membrane deformation and also
352 the least NOM fouling.



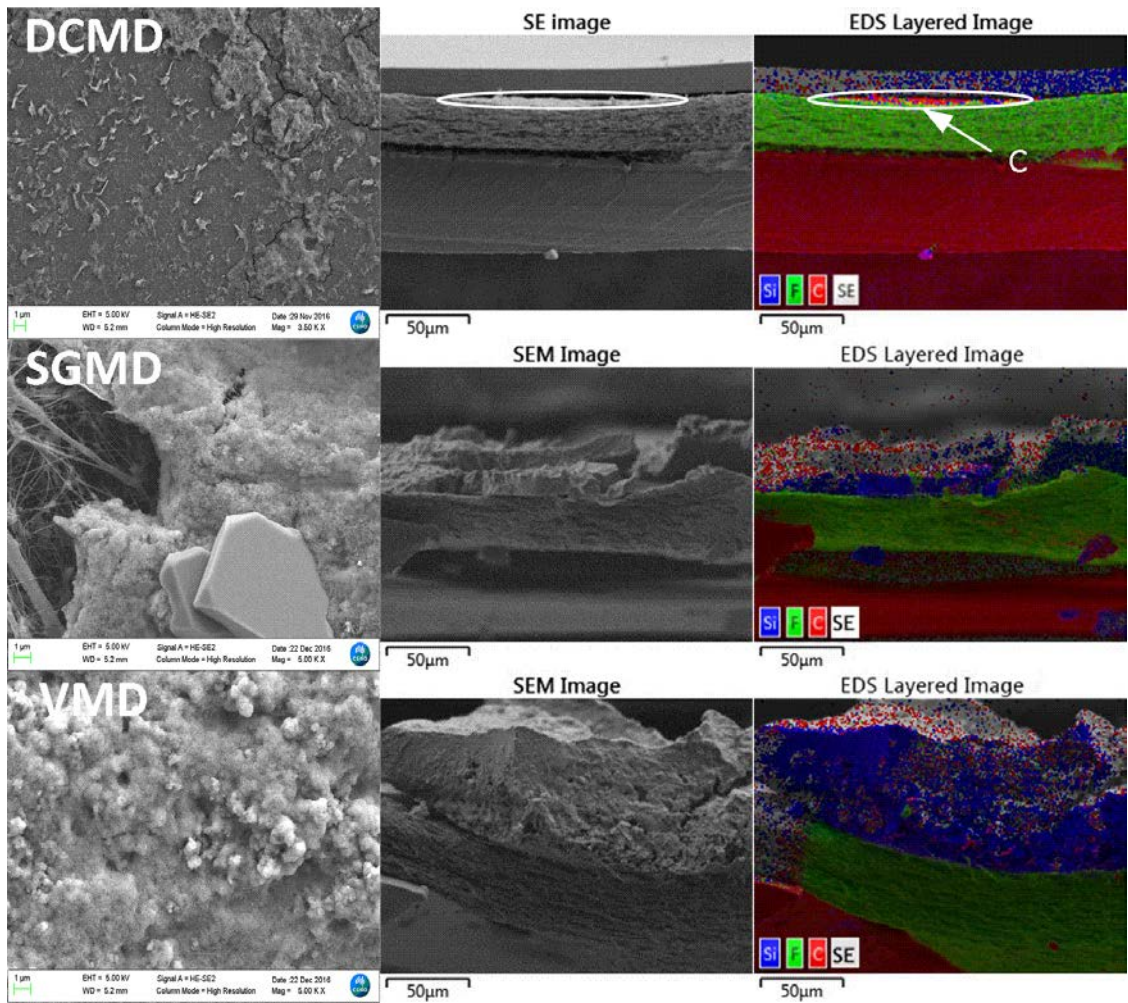
353

354 (a) Si



355

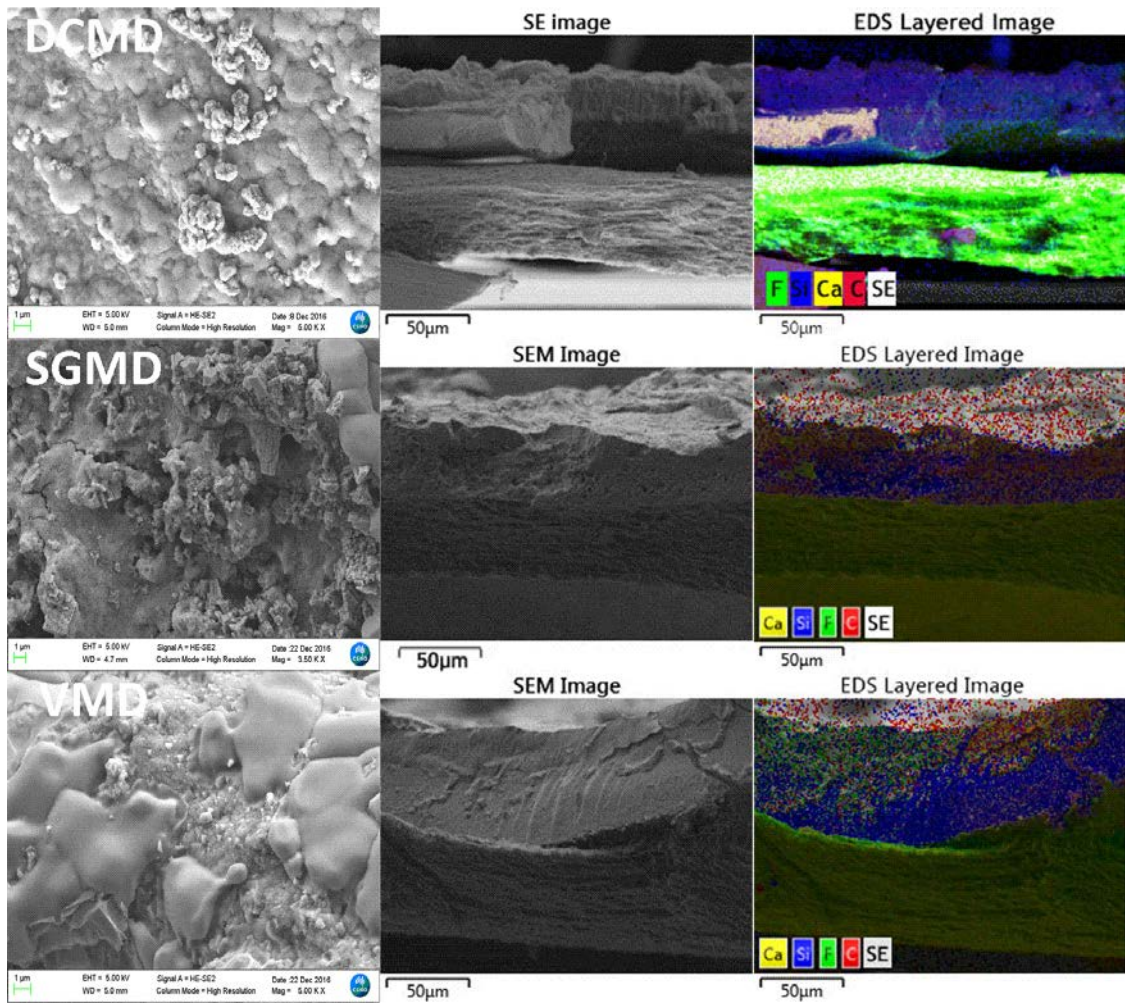
356 (b) Si+Ca



357

358 (c) Si+NOM

359



360

361 (d) Si+NOM+Ca

362 Figure 5. SEM and EDS he fouled membrane in different configuration: (a) Si, (b)

363 Si+Ca, (c) Si+NOM, (d) Si+NOM+Ca

364

365 The SEM images for the feed containing the Si+Ca+NOM are shown in Figure

366 5(d). Calcium carbonate scaling formed on top of the fouling layer for DCMD (Figure

367 5(d)) and the extent of deposited material appeared less than that of the Si+Ca feed,

368 which also corresponded to the flux decline that occurred at 24% recovery shown for

369 the DCMD curve in Figure 2(d). Furthermore, no crystal structure was observed for the

370 fouling layer surfaces in all configurations in Figure 5(d), and the boundary for different

371 foulants could not be easily identified compared to other foulant combinations, which
372 demonstrates the existence of interaction among the those foulants.

373 To understand the fouling behavior further, computational fluid dynamics (CFD)
374 and modelling of MD systems may be a useful addition to understanding the impact of
375 MD configuration on fouling performance. Furthermore, the XPS or other surface
376 characterization methods to autopsy the used MD membranes may also provide greater
377 insight as to the processes occurring.

378 **4. Conclusion**

379 Four different combinations of three foulants including Si, Si+Ca, Si+NOM and
380 Si+NOM+Ca were used in the study. The fouling behavior in DCMD, SGMD and
381 VMD were compared for up to 25% feed recovery.

382 Although DCMD showed the highest flux in all configurations, except for
383 Si+NOM+Ca combination. The combinations and interaction of the three foulants
384 showed higher dependence on membrane flux incurred concentration polarization than
385 turbulence and led to the worst fouling for DCMD process.

386 SGMD showed the best fouling resistance in all configurations because of its lower
387 flux and good hydrodynamic mixing of the feed side, although it was inclined to
388 calcium carbonate fouling due to the stripping of CO_2 from feed. However, this issue
389 can be alleviated by using air rather than pure nitrogen as the sweeping gas, since the
390 partial pressure of CO_2 in the air is not zero and will reduce the CO_2 depletion rate.

391 VMD almost showed the worst fouling resistance to most tested foulant

392 combinations due to the deformation of PTFE membrane under unbalanced pressure.
393 Wetting was also incurred in VMD by the combination of fouling and relative high
394 hydraulic pressure difference across the membrane. Therefore, the use of compressible
395 membrane in VMD process might increase particulate fouling. Furthermore, even if an
396 incompressible membrane was used, employing VMD in high-concentration calcium
397 bicarbonate or carbonate foulants still needs to be avoided when there is no scale
398 inhibitors

399 Based on the experimental conditions and results, it was found that the particulate
400 fouling could be reduced by avoiding dead zones (static zone) in the flow channel. To
401 alleviate NOM fouling, choosing an adequate flux to reduce the concentration
402 polarization will be more effective.

403 **5. Acknowledgement**

404 The authors would like to acknowledge the CSIRO Manufacturing for the financial
405 support of this work. W. Qin would like to thank the PhD student exchange scholarship
406 from Zhejiang University. Mr Mark Greaves from CSIRO Manufacturing is greatly
407 acknowledged for his help in SEM.

408

409

410

411 **Reference:**

412 Alklaibi, A.M. and Lior, N. (2005) Membrane-distillation desalination: Status and potential. *Desalination*
413 171(2), 111-131.

414 Bacchin, P., Aimar, P. and Field, R.W. (2006) Critical and sustainable fluxes: Theory, experiments and
415 applications. *Journal of Membrane Science* 281(1-2), 42-69.

416 Ballantyne, A.P., Alden, C.B., Miller, J.B., Tans, P.P. and White, J.W.C. (2012) Increase in observed net
417 carbon dioxide uptake by land and oceans during the past 50 years. *Nature* 488(7409), 70-72.

418 Banat, F., Jumah, R. and Garaibeh, M. (2002) Exploitation of solar energy collected by solar stills for
419 desalination by membrane distillation. *Renewable Energy* 25(2), 293-305.

420 Chen, V., Fane, A.G., Madaeni, S. and Wenten, I.G. (1997) Particle deposition during membrane filtration
421 of colloids: transition between concentration polarization and cake formation. *Journal of Membrane*
422 *Science* 125(1), 109-122.

423 Enríquez, O.R., Hummelink, C., Bruggert, G.-W., Lohse, D., Prosperetti, A., van der Meer, D. and Sun,
424 C. (2013) Growing bubbles in a slightly supersaturated liquid solution. *Review of scientific instruments*
425 84(6), 065111.

426 Frear, G. and Johnston, J. (1929) THE SOLUBILITY OF CALCIUM CARBONATE (CALCITE) IN
427 CERTAIN AQUEOUS SOLUTIONS AT 25° 1. *Journal of the American Chemical Society* 51(7), 2082-
428 2093.

429 Gajevskiy, V. (2015) Electric conductivity of carbon dioxide aqueous solutions. *Ukrainian journal of*
430 *physics* (60, № 3), 258-262.

431 Geankoplis, C.J. (2003) Transport processes and separation process principles Prentice Hall Press, Saddle
432 River.

433 Gryta, M. (2008) Fouling in direct contact membrane distillation process. *Journal of Membrane Science*
434 325(1), 383-394.

435 Kitano, Y., Kanamori, N. and Tokuyama, A. (1969) Effects of organic matter on solubilities and crystal
436 form of carbonates. *American Zoologist* 9(3), 681-688.

437 Laqbaqbi, M., Sanmartino, J., Khayet, M., García-Payo, C. and Chaouch, M. (2017) Fouling in
438 Membrane Distillation, Osmotic Distillation and Osmotic Membrane Distillation. *Applied Sciences* 7(4),
439 334.

440 Lawson, K.W., Hall, M.S. and Lloyd, D.R. (1995) Compaction of microporous membranes used in
441 membrane distillation. I. Effect on gas permeability. *Journal of Membrane Science* 101(1-2), 99-108.

442 Lawson, K.W. and Lloyd, D.R. (1997) Membrane distillation. *Journal of Membrane Science* 124(1), 1-
443 25.

444 Lee, N., Amy, G., Croué, J.-P. and Buisson, H. (2004) Identification and understanding of fouling in low-
445 pressure membrane (MF/UF) filtration by natural organic matter (NOM). *Water Research* 38(20), 4511-
446 4523.

447 Lei, Z., Chen, B. and Ding, Z. (2005) Special Distillation Processes. Lei, Z., Chen, B. and Ding, Z. (eds),
448 pp. 241-319, Elsevier Science, Amsterdam.

449 Light, T.S., Kingman, B. and Bevilacqua, A.C. (1995) The Conductivity of Low Concentrations of CO₂
450 Dissolved in Ultrapure Water from 0-100 C, pp. 2-6.

451 Mulder, M. (1996) Basic Principles of Membrane Technology, Kluwer, Dordrecht.

452 Phattaranawik, J., Jiratananon, R., Fane, A.G. and Halim, C. (2001) Mass flux enhancement using
453 spacer filled channels in direct contact membrane distillation. *Journal of Membrane Science* 187(1-2),
454 193-201.

455 Qin, W., Zhang, J., Xie, Z., Ng, D., Ye, Y., Gray, S.R. and Xie, M. (2017) Synergistic effect of combined

456 colloidal and organic fouling in membrane distillation: Measurements and mechanisms. *Environmental*
457 *Science: Water Research & Technology* 3(1), 119-127.

458 Rae, P.J. and Brown, E.N. (2005) The properties of poly(tetrafluoroethylene) (PTFE) in tension. *Polymer*
459 46(19), 8128-8140.

460 Rae, P.J. and Dattelbaum, D.M. (2004) The properties of poly(tetrafluoroethylene) (PTFE) in
461 compression. *Polymer* 45(22), 7615-7625.

462 Schneider, K. and van Gassel, T.J. (1984) Membrandestillation. *Chemie Ingenieur Technik* 56(7), 514-
463 521.

464 Trushina, D.B., Sulyanov, S.N., Bukreeva, T.V. and Kovalchuk, M.V. (2015) Size control and structure
465 features of spherical calcium carbonate particles. *Crystallography Reports* 60(4), 570-577.

466 Wang, Z., Elimelech, M. and Lin, S. (2016a) Environmental applications of interfacial materials with
467 special wettability. *Environmental Science & Technology* 50(5), 2132-2150.

468 Wang, Z., Hou, D. and Lin, S. (2016b) Composite membrane with underwater-oleophobic surface for
469 anti-oil-fouling membrane distillation. *Environmental Science & Technology* 50(7), 3866-3874.

470 Warsinger, D.M., Swaminathan, J., Guillen-Burrieza, E. and Arafat, H.A. (2015) Scaling and fouling in
471 membrane distillation for desalination applications: A review. *Desalination* 356, 294-313.

472 Weyl, P.K. (1967) Recovery of demineralized water from saline waters, U. S. A.

473 Yu, J., Lei, M. and Cheng, B. (2004) Facile preparation of monodispersed calcium carbonate spherical
474 particles via a simple precipitation reaction. *Materials Chemistry and Physics* 88(1), 1-4.

475 Zhang, J., Dow, N., Duke, M., Ostarcevic, E., Li, J.-D. and Gray, S. (2010a) Identification of material
476 and physical features of membrane distillation membranes for high performance desalination. *Journal of*
477 *Membrane Science* 349(1-2), 295-303.

478 Zhang, J., Duke, M., Hoang, M., Xie, Z., Groth, A., Tun, C. and Gray, S. (2013a) Influence of module
479 design and membrane compressibility on VMD performance. *Journal of Membrane Science* 442, 31-38.

480 Zhang, J., Gray, S. and Li, J.-D. (2012) Modelling heat and mass transfers in DCMD using compressible
481 membranes. *Journal of Membrane Science* 387-388(0), 7-16.

482 Zhang, J., Li, J.-D., Duke, M., Hoang, M., Xie, Z., Groth, A., Tun, C. and Gray, S. (2013b) Modelling of
483 vacuum membrane distillation. *Journal of Membrane Science* 434, 1-9.

484 Zhang, J., Li, J.-D., Duke, M., Xie, Z. and Gray, S. (2010b) Performance of asymmetric hollow fibre
485 membranes in membrane distillation under various configurations and vacuum enhancement. *Journal of*
486 *Membrane Science* 362(1), 517-528.

487 Zhang, J., Li, J.-D. and Gray, S. (2011) Effect of applied pressure on performance of PTFE membrane in
488 DCMD. *Journal of Membrane Science* 369(1), 514-525.

489